Journal of Applied Geophysics 109 (2014) 7–14

Contents lists available at ScienceDirect

Journal of Applied Geophysics

journal homepage: www.elsevier.com/locate/jappgeo

Gaussian beam prestack depth migration of converted wave in TI media

Jianguang Han [a,b,*], Yun Wang [c], Zhantao Xing [a], Jun Lu [d]

[a] Institute of Geology and Geophysics, Chinese Academy of Sciences, Beijing 100029, China
[b] University of Chinese Academy of Sciences, Beijing 100049, China
[c] Institute of Geochemistry, Chinese Academy of Sciences, Guiyang 550002, China
[d] China University of Geosciences (Beijing), Beijing 100083, China

ARTICLE INFO

Article history:
Received 26 February 2014
Accepted 7 July 2014
Available online 15 July 2014

Keywords:
Transversely isotropy media
Converted wave
Ray tracing
Gaussian beam prestack depth migration

ABSTRACT

Increasing amounts of multi-component seismic data are being acquired on land and offshore because more complete seismic wavefield information is beneficial for structural imaging, fluid detection, and reservoir monitoring. S-waves are typically influenced more by anisotropy in a medium than are P-waves; as a result, the anisotropy cannot be ignored during the converted PS-wave imaging. Gaussian beam migration, an elegant and efficient depth migration method, is becoming a new topic in the study of PS-wave migration; its accuracy is comparable to that of wave-equation migration, and its flexibility is comparable to that of Kirchhoff migration. In this paper, we introduce an anisotropic Gaussian beam prestack depth migration (GB-PSDM) method for the converted PS-wave, in which the anisotropic media can be a transversely isotropic (TI) medium with a vertical or tilted symmetry axis. We present the PS-wave common shot gathers GB-PSDM imaging condition and derive the ray tracing of P- and SV-waves in two-dimensional TI media. The migration impulse responses of P- and SV-propagation modes in TI media with both vertical and tilted symmetry axes are presented. The results of numerical examples indicate that the method introduced here offers significant improvements in the quality of converted PS-wave imaging compared with an isotropic algorithm.

1. Introduction

Multi-component seismic technology, specifically converted PS-wave technology, has been developing rapidly in recent years. More complete seismic wavefield information can be acquired using multi-component seismic technology, which is beneficial for structural imaging, lithology estimation and anisotropy analysis, fluid detection, and reservoir monitoring (Stewart et al., 2002, 2003); such tasks are important in many aspects of reservoir exploration, characterization and exploitation.

The key problem of the application of multi-component technology is PS-wave data processing. The major complexity in processing PS-wave data is the asymmetry of the source-to-receiver ray paths. Because the zero-dip conversion point locations change substantially from top to bottom of a converted-wave seismic trace, the regular processing flow of NMO plus DMO and poststack migration can have difficulty achieving an optimal image. The prestack time migration is a good choice for converted wave imaging (Bancroft et al., 1998; Wang et al., 2012). However, in areas where the geological structures are complex and the velocity variations are substantial, the prestack depth migration would be more desirable (Miao et al., 2005). Several case studies regarding the isotropic prestack depth migration of converted PS-wave data illustrated the benefits of performing imaging in depth rather than imaging in time (e.g., Kendall et al., 1998; Sun and McMechan, 2001; Xie and Wu, 2005; Zhu et al., 1999).

The earth is anisotropic in nature, and many sedimentary rocks have been found to be anisotropic in experiments (Ball, 1995; Crampin et al., 1984; Levin, 1979; Thomsen, 1986; Wang, 2002; White et al., 1983). To a good and practical approximation, these sedimentary rocks can be described as being transversely isotropic (TI) with a symmetry axis perpendicular to the bedding plane (Zhang et al., 2001). Seismic waves are affected by anisotropy, so ignoring anisotropy in migration may result in large positional errors or a complete loss of steeply dipping structures (Alkhalifah and Larner, 1994; Isaac and Lawton, 1999; Kumar et al., 2004; Larner and Cohen, 1993; Vestrum et al., 1999; Zhang et al., 2011).

Because S-waves are typically more influenced by anisotropy in a medium than are P-waves (Thomsen, 1999), the anisotropy of the medium cannot be ignored in converted PS-wave image. Several researchers have studied the anisotropic prestack time migration for converted PS-wave imaging (e.g., Dai and Li, 2006; Li et al., 2007; Miao and Torre, 2007; Sun and Martinez, 2003; Wang et al., 2002; Zhang and Liu, 2008). In addition, anisotropic prestack depth migration methods of converted PS-wave have also been studied by several researchers. Sena and Toksöz (1993) extended the isotropic Kirchhoff depth migration scheme to the anisotropic case for non-converted and converted PS-waves by using anisotropic ray tracing. Han (2000) proposed two prestack depth

* Corresponding author at: Institute of Geology and Geophysics, Chinese Academy of Sciences, Beijing 100029, China.
E-mail address: hanjianguang@mail.iggcas.ac.cn (J. Han).

http://dx.doi.org/10.1016/j.jappgeo.2014.07.008
0926-9851/

migration algorithms of converted PS-wave in VTI media, including anisotropic phase-shift-plus-interpolation (PSPI) and anisotropic implicit finite-difference (FD) algorithms. Nolte (2005) described a technique for converted-wave migration in anisotropic media with VTI symmetry using Fourier finite-difference (FFD) methods through least-squares fitting of the finite difference coefficients to an anisotropic dispersion relation. Du et al. (2007) derived the P- and SV-wave equations for TTI media and presented impulse responses of P- and SV-waves in TTI media with different tilt angles. Pedersen et al. (2010) derived phase-slowness expressions for P- and SV-waves that are used in a one-way wave-equation migration scheme in VTI media.

Common for all of the depth imaging studies mentioned above is that the imaging methods are based on Kirchhoff migration and wave-equation migration. The Kirchhoff migration method is more efficient and flexible, but it has multi-valued traveltimes, which affect the migration result. Wave-equation based migration techniques might provide better solutions to the imaging of converted wave than the Kirchhoff techniques. However, the wave-equation based method is very time consuming. Gaussian beam migration, a powerful imaging technique, is an elegant and efficient depth migration method, with an accuracy comparable to that of wave-equation migration and a flexibility comparable to that of Kirchhoff migration (Gray and Bleistein, 2009).

In the field of seismology, the Gaussian beam method for the computation of wavefield (Červeny et al., 1982, 2007; Popov, 1982) was first used in the seismic wavefield forward modeling (Červeny, 1985; Nowack, 2003), followed by the study of the Gaussian beam migration method. Hill (1990) proposed a Gaussian beam poststack migration method and performed a detailed study of the migration parameters. Hale (1992a,b) further introduced an algorithm and implementation of Gaussian beam migration. Hill (2001) presented a prestack Gaussian beam migration method in isotropic media that operates on common-offset and common-azimuth data volumes. Gray (2005) removed the narrow azimuth restriction by presenting variations suitable for common-shot record migration. In subsequent publications, true-amplitude Gaussian-beam migration methods were developed by Gray and Bleistein (2009) and Popov et al. (2008, 2010). Meanwhile, Gaussian beam depth migration in anisotropic media was studied. Alkhalifah (1995) first proposed a Gaussian beam poststack depth migration method for anisotropic media. Zhu et al. (2007) presented a prestack Gaussian beam depth migration method in anisotropic media and applied it with encouraging results to synthetic data. However, these studies of Gaussian beam migration are only applied to acoustic wave migration. Casasanta et al. (2013) described a converted wave Gaussian beam migration method for TTI media and applied it with encouraging result to a synthetic data example.

In this paper, a method for anisotropic Gaussian beam prestack depth migration (GB-PSDM) of converted wave is presented. The goal here is to develop 2D prestack converted wave algorithms for depth migration in TI media. Unlike the method of Casasanta et al. (2013), our method is based on anisotropic ray tracing. We derive the ray tracing of P- and SV-waves for two-dimensional TI media, and a series of impulse responses of P- and SV-propagation modes in different TI models are presented. The accuracy and effectiveness of our migration algorithm are tested on synthetic examples.

2. Converted wave GB-PSDM imaging condition in anisotropic media

In this study, the cross-correlation imaging condition is used. The image of anisotropic GB-PSDM is formed by cross-correlating the downward-continued wavefields from the source and beam centers, which is the same as GB-PSDM in isotropic media. The central rays of the Gaussian beam are emitted from the source and beam centers with different ray parameters to compute the wavefields. For the PS-wave image, downward-continued source wavefields are computed with the P-wave, and the S-wave is used to compute the wavefields from the beam center points, as shown in Fig. 1.

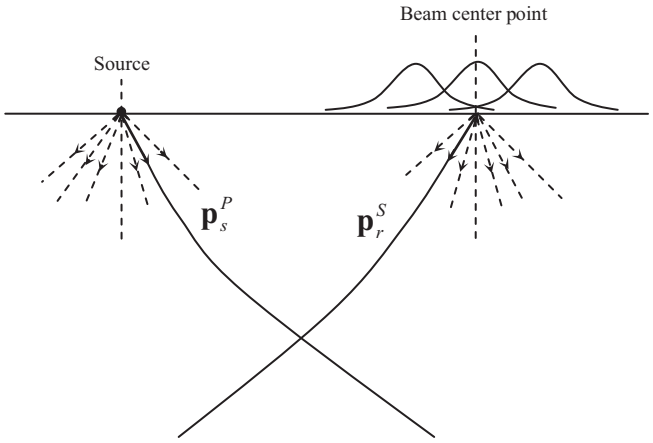

Fig. 1. Sketch of PS-wave Gaussian beam prestack depth migration. The P-wave is used to compute the wavefields from the source with ray parameters $\mathbf{p}_s^P$ and the S-wave is used to compute the wavefields from beam center points with ray parameters $\mathbf{p}_r^S$.

In a two-dimensional anisotropic media, assume that $\mathbf{x}_s = (x_s, 0)$ and $\mathbf{x}_r = (x_r, 0)$ denote the source and receiver locations. According to the Gaussian beam prestack migration method that operates on common-offset gathers given by Hill (2001), the PS-wave common shot gathers Gaussian beam migration formula can be written as

$$I^{PS}(\mathbf{x}) = C^{PS}\int dx_s \sum_{L_r}\int d\omega \int dp_{sx}^P \int dp_{rx}^S D^{PS}\left(\mathbf{L}_r, \mathbf{p}_r^S, \omega\right) \times u_{GB}^{P*}\left(\mathbf{x}, \mathbf{x}_s, \mathbf{p}_s^P, \omega\right) u_{GB}^{S*}\left(\mathbf{x}, \mathbf{L}_r, \mathbf{p}_r^S, \omega\right) \tag{1}$$

where $I^{PS}(\mathbf{x})$ is the PS-wave final image at subsurface point $\mathbf{x} = (x,z)$, ω is the circular frequency, and C^{PS} denotes corresponding constant. $u_{GB}^{P*}(\mathbf{x}, \mathbf{x}_s, \mathbf{p}_s^P, \omega)$ and $u_{GB}^{S*}(\mathbf{x}, \mathbf{L}_r, \mathbf{p}_r^S, \omega)$ are the complex conjugates of the normalized Gaussian beam solutions of P- and S-waves to the wave-equation, where the former represents P-wave propagation from source $\mathbf{x}_s$ with initial direction $\mathbf{p}_s^P$, and the latter signifies S-wave propagation from the beam center $\mathbf{L}_r$ with initial direction $\mathbf{p}_r^S$. $D^{PS}(\mathbf{L}_r, \mathbf{p}_r^S, \omega)$ is the local plane wave component obtained from a local slant stack of the PS-wave common-shot traces, and the expression can be written as

$$D^{PS}\left(\mathbf{L}_r, \mathbf{p}_r^S, \omega\right) = \frac{1}{4\pi^2}\left|\frac{\omega}{\omega_r}\right|^3 \int dx_r u^{PS}(\mathbf{x}_r, \mathbf{x}_s, \omega) \times \exp\left[-i\omega p_{rx}^S(x_r - L_r) - \frac{1}{2}\left|\frac{\omega}{\omega_r}\right|\frac{|x_r - L_r|^2}{L_0^2}\right] \tag{2}$$

where ω_r is the reference frequency, and $u^{PS}(\mathbf{x}_r, \mathbf{x}_s, \omega)$ is the recorded wavefield of the PS-wave. $L_0 = \frac{v_{avg}}{f_{min}}$ is the initial beam width, where f_{min} is the minimum frequency, and v_{avg} is the average of the horizontal and vertical velocities over the entire grid (Alkhalifah, 1995).

If functions A and T are used to represent complex amplitude and traveltime, respectively, of the Gaussian beam, then the Gaussian beam expression can be written as

$$u_{GB}(\mathbf{x}, \mathbf{x_0}, \mathbf{p}, \omega) = A\exp(i\omega T). \tag{3}$$

Inserting the corresponding P- and S-wave Gaussian beam expressions into Eq. (1), it can be rewritten as

$$I^{PS}(\mathbf{x}) = C^{PS}\int dx_s \sum_{L_r}\int d\omega D^{PS}\left(\mathbf{L}_r, \mathbf{p}_r^S, \omega\right) \times \int dp_{sx}^P \int dp_{rx}^S \overline{A}^{PS}\left(\mathbf{x}, \mathbf{p}_s^P, \mathbf{p}_r^S\right) \exp\left[-i\omega \overline{T}^{PS}\left(\mathbf{x}, \mathbf{p}_s^P, \mathbf{p}_r^S\right)\right] \tag{4}$$

where function $\overline{A}^{PS}\left(\mathbf{x},\mathbf{p}_s^P,\mathbf{p}_r^S\right)$ is the product of the amplitudes of the beams from the source and beam centers; $\overline{T}^{PS}\left(\mathbf{x},\mathbf{p}_s^P,\mathbf{p}_r^S\right)$ is the PS-wave complex traveltime determined by the beams from the source and beam centers, and

$$\overline{T}^{PS}\left(\mathbf{x},\mathbf{p}_s^P,\mathbf{p}_r^S\right)=T_{\mathbf{x}_s}^P\left(\mathbf{x},\mathbf{p}_s^P\right)+T_{\mathbf{L}_r}^S\left(\mathbf{x},\mathbf{p}_r^S\right) \tag{5}$$

where $T_{\mathbf{x}_s}^P\left(\mathbf{x},\mathbf{p}_s^P\right)$ and $T_{\mathbf{L}_r}^S\left(\mathbf{x},\mathbf{p}_r^S\right)$ are the complex traveltimes for the beams coming from the source and beam centers computed with P- and S-waves, respectively.

Gaussian beam migration requires the proper choice of several important parameters, such as the initial beam width and the spacing of beams and ray parameters, to guarantee the quality of migration imaging. These computational formulas of parameters used in our anisotropic GB-PSDM are similar to those given by Alkhalifah (1995). Compared with the PP-wave, it has polarity reversal problem on the PS-wave seismic record, and direct migration for the PS-wave will seriously affect the migration result. Therefore, based on the polarity characteristics of the PS-wave records, the polarity has been corrected in the process of Gaussian beam prestack depth migration.

3. Anisotropic ray tracing

The calculations of the complex amplitude and traveltime of Gaussian beam require anisotropic kinematic and dynamic ray tracing, which is the key of the anisotropic GB-PSDM. In two dimensions along a symmetry plane, all of the out-of-plane components are eliminated, namely, all components with subscript 2, so only P- and SV-waves are considered. The anisotropic ray tracing theory derived by Červeny (1972, 2001) can be used quite universally for P- and SV-waves in two-dimensional media. It can be written in two-dimensional TI media as

$$\begin{aligned}\frac{dx_1}{d\tau}=&a_{11}p_1g_1^{(m)}g_1^{(m)}+a_{15}p_3g_1^{(m)}g_1^{(m)}+2a_{15}p_1g_1^{(m)}g_3^{(m)}+a_{13}p_3g_1^{(m)}g_3^{(m)}\\&+a_{55}p_3g_1^{(m)}g_3^{(m)}+a_{55}p_1g_3^{(m)}g_3^{(m)}+a_{35}p_3g_3^{(m)}g_3^{(m)}\end{aligned} \tag{6a}$$

$$\begin{aligned}\frac{dx_3}{d\tau}=&a_{15}p_1g_1^{(m)}g_1^{(m)}+a_{55}p_3g_1^{(m)}g_1^{(m)}+a_{55}p_1g_1^{(m)}g_3^{(m)}+2a_{35}p_3g_1^{(m)}g_3^{(m)}\\&+a_{13}p_1g_1^{(m)}g_3^{(m)}+a_{35}p_1g_3^{(m)}g_3^{(m)}+a_{33}p_3g_3^{(m)}g_3^{(m)}\end{aligned} \tag{6b}$$

$$\begin{aligned}\frac{dp_1}{d\tau}=&-\frac{1}{2}\left(\frac{\partial a_{11}}{\partial x_1}p_1p_1g_1^{(m)}g_1^{(m)}+2\frac{\partial a_{15}}{\partial x_1}p_1p_3g_1^{(m)}g_1^{(m)}+2\frac{\partial a_{15}}{\partial x_1}p_1p_1g_1^{(m)}g_3^{(m)}\right.\\&+2\frac{\partial a_{13}}{\partial x_1}p_1p_3g_1^{(m)}g_3^{(m)}+2\frac{\partial a_{55}}{\partial x_1}p_1p_3g_1^{(m)}g_3^{(m)}+\frac{\partial a_{55}}{\partial x_1}p_1p_1g_3^{(m)}g_3^{(m)}\\&+2\frac{\partial a_{35}}{\partial x_1}p_1p_3g_3^{(m)}g_3^{(m)}+\frac{\partial a_{55}}{\partial x_1}p_3p_3g_1^{(m)}g_1^{(m)}+2\frac{\partial a_{35}}{\partial x_1}p_3p_3g_1^{(m)}g_3^{(m)}\\&\left.+\frac{\partial a_{33}}{\partial x_1}p_3p_3g_3^{(m)}g_3^{(m)}\right)\end{aligned} \tag{6c}$$

$$\begin{aligned}\frac{dp_3}{d\tau}=&-\frac{1}{2}\left(\frac{\partial a_{11}}{\partial x_3}p_1p_1g_1^{(m)}g_1^{(m)}+2\frac{\partial a_{15}}{\partial x_3}p_1p_3g_1^{(m)}g_1^{(m)}+2\frac{\partial a_{15}}{\partial x_3}p_1p_1g_1^{(m)}g_3^{(m)}\right.\\&+2\frac{\partial a_{13}}{\partial x_3}p_1p_3g_1^{(m)}g_3^{(m)}+2\frac{\partial a_{55}}{\partial x_3}p_1p_3g_1^{(m)}g_3^{(m)}+\frac{\partial a_{55}}{\partial x_3}p_1p_1g_3^{(m)}g_3^{(m)}\\&+2\frac{\partial a_{35}}{\partial x_3}p_1p_3g_3^{(m)}g_3^{(m)}+\frac{\partial a_{55}}{\partial x_3}p_3p_3g_1^{(m)}g_1^{(m)}+2\frac{\partial a_{35}}{\partial x_3}p_3p_3g_1^{(m)}g_3^{(m)}\\&\left.+\frac{\partial a_{33}}{\partial x_3}p_3p_3g_3^{(m)}g_3^{(m)}\right)\end{aligned} \tag{6d}$$

where the index m specifies the type of elementary wave under consideration. We use $m=1$ for the P-wave and $m=2$ for the SV-wave. $p_i=\frac{\partial\tau}{\partial x_i}(i=1,3)$ are the components of the slowness vector, $a_{mn}=c_{mn}/\rho(m,n=1,3,\text{ or }5)$ are the density-normalized elastic parameters, and $g_j^{(m)}(j=1,3)$ are the components of the eigenvector for the Christoffel matrix $\mathbf{\Gamma}$. The product of eigenvectors is given by (Alkhalifah, 1995; Červeny, 2001)

$$\begin{aligned}g_1^{(m)}g_1^{(m)}&=\frac{\Gamma_{33}-1}{\Gamma_{11}+\Gamma_{33}-2},\\g_3^{(m)}g_3^{(m)}&=\frac{\Gamma_{11}-1}{\Gamma_{11}+\Gamma_{33}-2},\\g_1^{(m)}g_3^{(m)}&=\frac{-\Gamma_{13}}{\Gamma_{11}+\Gamma_{33}-2}.\end{aligned} \tag{7}$$

The Christoffel matrix $\Gamma_{ik}=a_{ijkl}p_jp_l(i,j,k,l=1,3)$ contains the components of slowness vector (Červeny, 2001), which has been broadly used in the ray method of seismic waves propagating in inhomogeneous anisotropic media because it is very suitable for the study of the ray method.

The ray tracing system (6) is quite similar for P- and SV-waves, which can propagate in an anisotropic inhomogeneous media. The type of wave whose ray is to be computed is specified by the initial conditions, which must satisfy the eikonal equation of the considered wave. Thus, the initial conditions for the ray tracing system play an important role in the calculation of rays. The initial conditions not only specify the initial point and the initial direction of the ray but also the type of wave that is to be computed. The initial conditions for ray tracing system (6) are expressed as follows

$$x_i=x_{i0},p_i=p_{i0} \tag{8}$$

where the initial values of x_{i0} and p_{i0} must satisfy the eikonal equation, corresponding to the particular wave we wish to compute

$$G_m(x_{i0},p_{i0})=1. \tag{9}$$

Once eikonal Eq. (9) is satisfied at the initial point, the ray tracing system (6) keeps the eikonal equation satisfied along the entire ray. If the initial conditions (Eq. (8)) satisfying the eikonal Eq. (9) of the considered wave (P-wave or SV-wave) is known, the ray tracing system (6) for the corresponding seismic ray can be solved.

In two-dimensional media, eliminating all components with subscript 2, the expression for G_m can be rewritten as follows

$$G_m=\Gamma_{11}g_1^{(m)}g_1^{(m)}+2\Gamma_{13}g_1^{(m)}g_3^{(m)}+\Gamma_{33}g_3^{(m)}g_3^{(m)}. \tag{10}$$

Inserting Eq. (7) and the eikonal equation $G_m=1$ into Eq. (10), we obtain

$$(\Gamma_{11}-1)(\Gamma_{33}-1)-\Gamma_{13}^2=0. \tag{11}$$

Inserting the Christoffel matrix into Eq. (11), we can obtain a quartic equation of p_1 and p_3, which can be used to solve the initial vertical ray parameter p_3 for each initial ray parameter p_1.

For anisotropic media, the wavefield energy does not propagate in the direction of the phase-velocity vector, and the rays are not perpendicular to wavefronts. The ray-centered coordinates are no longer orthogonal as they are in isotropic media, so the dynamic ray tracing is more complicated in anisotropic media. The anisotropic dynamic ray tracing equations given by Hanyga (1986) is used in our anisotropic GB-PSDM, which is the same as that used by Alkhalifah (1995).

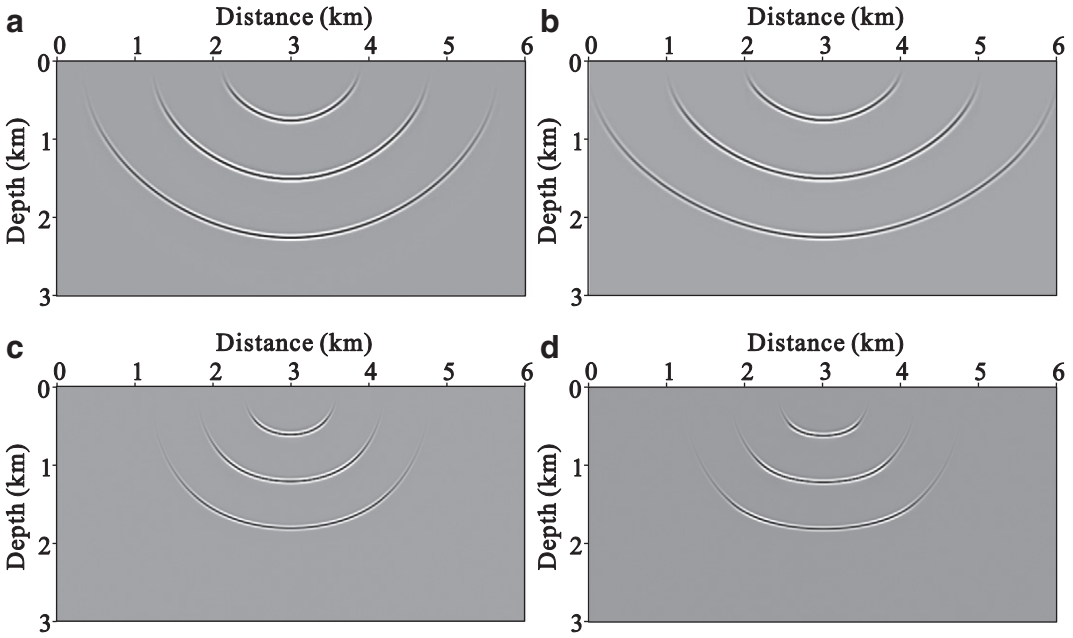

Fig. 2. Impulse responses using anisotropic GBM for P and SV modes in a VTI medium. The vertical velocity of the P-wave is 2500 m/s and that of the SV-wave is 2000 m/s. (a) and (b) are impulse responses of the P propagation mode, (c) and (d) of the SV mode. The Thomsen parameters are $\varepsilon = 0.2$ and $\delta = 0.1$ for (a) and (c), and $\varepsilon = 0.4$ and $\delta = 0.2$ for (b) and (d).

4. The elastic parameters of the TI media

A TI medium with a vertical axis of symmetry (VTI) is widely observed in sedimentary basins and is commonly used in exploration seismology. Only five independent elastic constants (c_{11}, c_{33}, c_{44}, c_{66}, and c_{13}) are required to describe the VTI model. Because the physical meaning of elastic constants is not straightforward, Thomsen (1986) introduced a set of parameters to describe the anisotropy, which facilitate the research of the anisotropic media and better reveal the physical meaning of the anisotropic parameters. The Thomsen parameters are expressed in terms of the elastic constants of the VTI media as

$$V_{P0} = \sqrt{\frac{c_{33}}{\rho}}, V_{S0} = \sqrt{\frac{c_{44}}{\rho}},$$
$$\varepsilon = \frac{c_{11} - c_{33}}{2c_{33}}, \delta = \frac{(c_{13} + c_{44})^2 - (c_{33} - c_{44})^2}{2c_{33}(c_{33} - c_{44})}, \gamma = \frac{c_{66} - c_{44}}{2c_{44}} \tag{12}$$

where ρ is the density; V_{P0} and V_{S0} are the phase velocities of P- and SV-waves along the symmetry axis of VTI media, respectively; and ε,

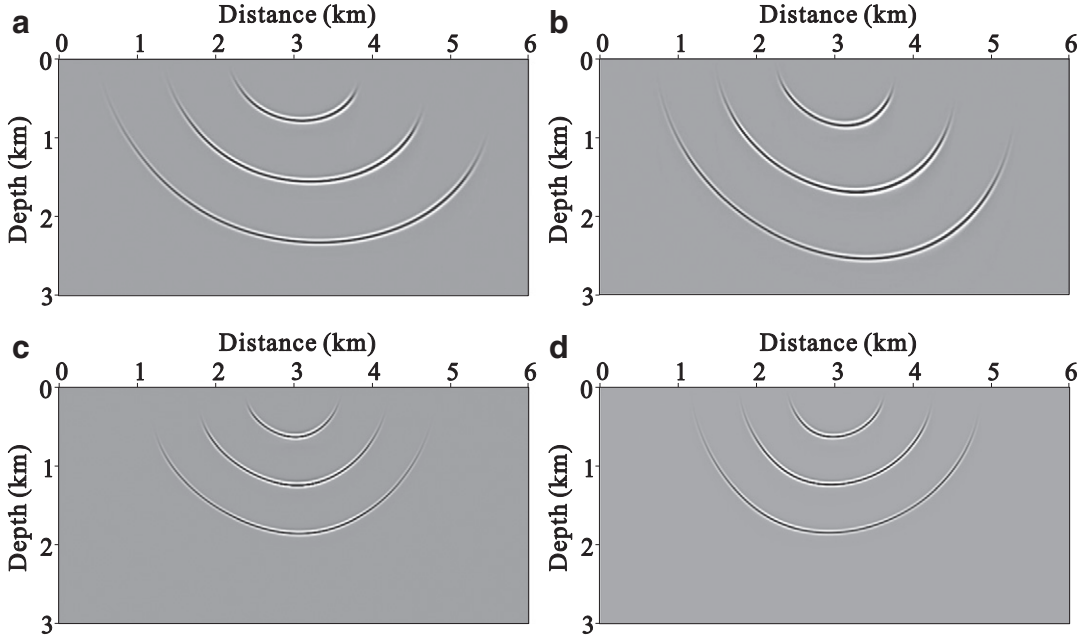

Fig. 3. Impulse responses of P and SV propagation modes in a TTI medium with Thomsen anisotropy parameters $\varepsilon = 0.2$ and $\delta = 0.1$. The vertical velocity of the P-wave is 2500 m/s and that of the SV-wave is 2000 m/s. (a) and (b) are impulse responses of the P propagation mode, (c) and (d) of the SV mode. The tilt angles are 30° for (a) and (c), and 60° for (b) and (d).

δ and γ are the three dimensionless anisotropic parameters that characterize the magnitude of the anisotropy. The parameter ε represents the anisotropy of the P-wave. The parameter δ governs the P-wave velocity variation away from the symmetry axis and also influences the SV-wave velocity (Tsvankin et al., 2010). The parameter γ determines the SH-wave, which is not discussed in this paper, so it need not be considered here.

The density-normalized elastic parameters are used in this paper. According to the relationship between the Thomsen parameters and the elastic constants, the density-normalized elastic constants can be expressed using the Thomsen parameters as

$$\begin{aligned} &a_{11} = (1+2\varepsilon)V_{P0}^2, a_{33} = V_{P0}^2, \\ &a_{44} = a_{55} = V_{S0}^2, a_{66} = (1+2\gamma)V_{S0}^2, \\ &a_{13} = \sqrt{2\delta a_{33}(a_{33}-a_{44}) + (a_{33}-a_{44})^2} - a_{44}. \end{aligned} \tag{13}$$

When elastic boundaries in the subsurface are dipping, the symmetry axis of TI media may not be vertical. Such media are referred to as TI media with a tilted symmetry axis (TTI). In this paper, the angle between the symmetry axis and the vertical direction is denoted as θ^0 for TTI media. The elastic constants of TTI media can be obtained from the ones of the VTI media via the Bond transformation (Winterstein, 1990).

5. Numerical examples

5.1. Impulse response

In this section, a series of migration impulse responses of P- and SV-propagation modes in TI media with both vertical and tilted symmetry axes are presented. The model is defined on a 601 × 301 grid with a grid spacing of 10 m. A single input trace is located at the center of the upper surface, which contains three impulses located at times 0.6, 1.2, and 1.8 s. A Ricker wavelet with a dominant frequency of 20 Hz is used to generate the impulse response. The vertical velocity of the P-wave is 2500 m/s, and that of the SV-wave is 2000 m/s. An imaging angle in the range of −80° to 80° is used for migration of the P- and SV-waves.

Fig. 2 illustrates impulse responses of P- and SV-propagation modes in a VTI medium for both weak and strong anisotropy cases. We take $\varepsilon = 0.2$ and $\delta = 0.1$ as an example of a weak anisotropy and $\varepsilon = 0.4$ and $\delta = 0.2$ as an example of a strong anisotropy. Fig. 3 shows the impulse responses of the P- and SV-propagation modes in a TTI medium with tilt angles of 30° and 60°. The Thomsen anisotropy parameters of this TTI medium are $\varepsilon = 0.2$ and $\delta = 0.1$. Considering the anisotropy effect, the wavefronts of P- and SV-waves are very different from the circular ones of an isotropic medium, especially for the SV-wave. Based on these calculations, we conclude that the impulse responses exhibit good kinematic behavior for both P migration and SV migration. The good imaging quality in Figs. 2 and 3 demonstrates the effectiveness of our migration method proposed here.

5.2. Test on strongly VTI media

To verify the accuracy of our anisotropic converted-wave Gaussian beam prestack depth migration method, we tested our method on a strong VTI media model with different anisotropic parameters in each layer, as shown in Fig. 4. The PS-wave synthetic dataset is generated using the anisotropic ray tracing forward modeling method, and the source wavelet is the Ricker wavelet with a dominant frequency of 30 Hz. There are 77 shots on the surface with 401 receivers per shot. The shot spacing is 50 m, and the receiver spacing is 10 m. The traveltime is 3 s, with 2 ms of sampling.

Fig. 5a displays the resulting image of PS-wave using isotropic GB-PSDM without considering the effect of anisotropy, where the image of the synclinal structure is not accurate. The noise is significant near

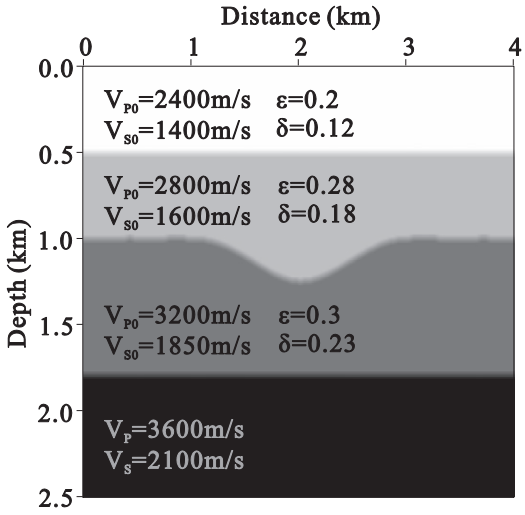

Fig. 4. Subsurface VTI media model with different anisotropy parameters in each layer.

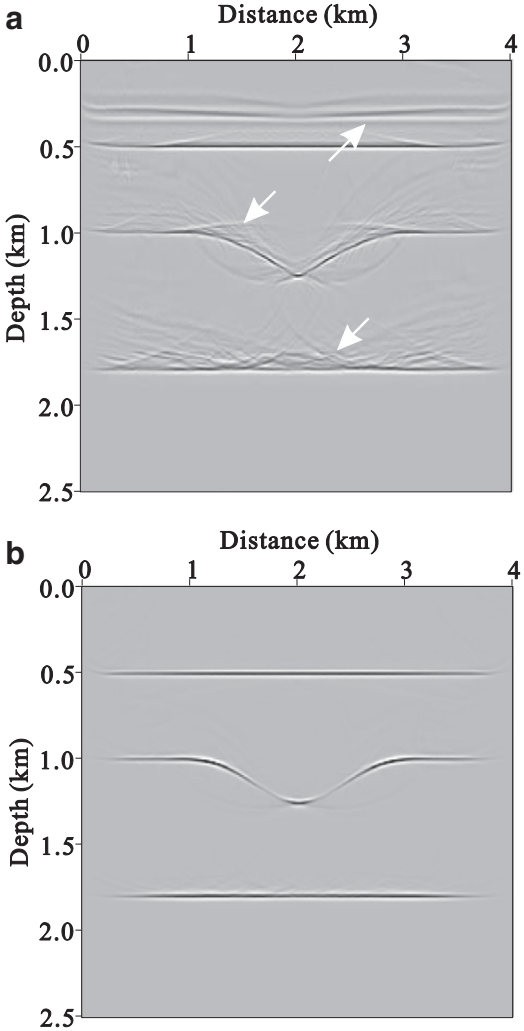

Fig. 5. Migration results of VTI media model shown in Fig. 3. (a) Isotropic GB-PSDM result of converted PS-wave. The P-wave velocity $V_P = V_{P0}$ and SV-wave velocity $V_S = V_{S0}$ are used, without considering the effect of Thomsen parameters ε and δ. (b) Anisotropic GB-PSDM result of converted PS-wave. The exact velocity model and Thomsen parameters have been applied. The migration result exactly matches the true interfaces.

the reflection interfaces, and defocusing artifacts are obvious around the synclinal structure, as indicated by the arrow in Fig. 5a. Fig. 5b shows the anisotropic GB-PSDM result with the correct media parameters and velocity values. The migration result is found to be an excellent match with the exact model interface, and the defocusing artifacts are eliminated. Clearly, the image in Fig. 5b is superior to that in Fig. 5a. To further display the influence of anisotropy on the converted PS-wave migration, the corresponding converted PS-wave CIGs located at 2800 m from the isotropic and anisotropic GB-PSDM are shown in Fig. 6a and b, respectively. By comparing Fig. 6a with b, the converted PS-wave CIGs computed with isotropic GB-PSDM are found to be not flat because the effect of anisotropic parameters ε and δ was ignored. In contrast, the CIGs extracted from the anisotropic GB-PSDM are flat, and the depths of the events in the CIGs are correct. These observations verify that the proposed anisotropic converted PS-wave GB-PSDM in strong VTI media is effective.

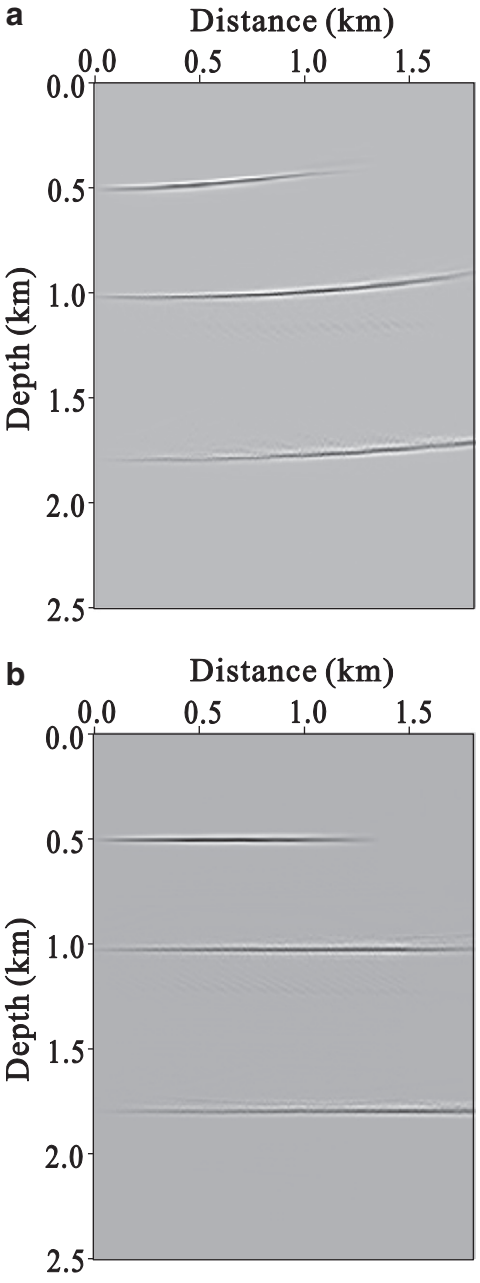

Fig. 6. Converted PS-wave CIGs at 2800 m from (a) isotropic GB-PSDM and (b) anisotropic GB-PSDM.

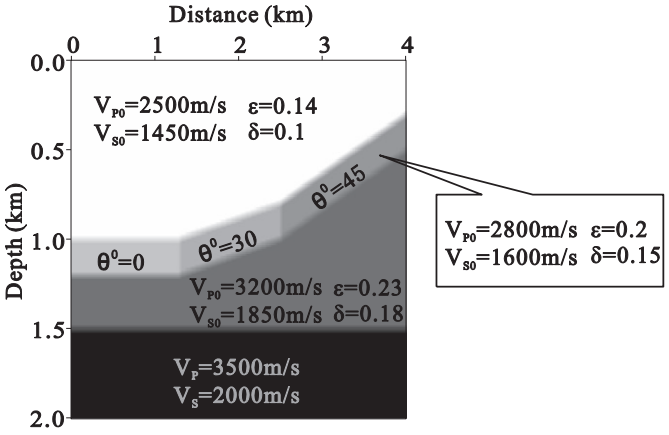

Fig. 7. Subsurface TTI media model including a flat reflector and a TTI thrust sheet. The thrust sheet is composed of three blocks in the model, and it has a spatially varying symmetry axis.

5.3. Test on TTI media

Next, the accuracy of our anisotropic converted-wave Gaussian beam prestack depth migration method is demonstrated on a TTI media model. The model contains a flat reflector and a TTI thrust sheet, as shown in Fig. 7. The first and third layers are VTI media with different anisotropic parameters. The thrust sheet has a spatially varying symmetry axis. The PS-wave synthetic dataset is generated using the anisotropic ray tracing forward modeling method, and the source wavelet is the Ricker wavelet with a dominant frequency of 30 Hz. There are 39 shots on the surface, with 401 receivers per shot. The shot spacing is 100 m, and the receiver spacing is 10 m. The traveltime is 3 s, with 2 ms of sampling.

Fig. 8a and b shows the resulting images of PS-wave using isotropic and anisotropic GB-PSDM, respectively. The P-wave velocity $V_P = V_{P0}$ and SV-wave velocity $V_S = V_{S0}$ are used for the isotropic GB-PSDM. The resulting image (Fig. 8a) indicates that the flat reflector beneath the thrust sheet exhibits a spurious pull-up and that the energy cannot be focused. The dipping interface of the thrust sheet is not imaged at the true position, and some defocusing effects along the thrust sheet are also visible. The image obtained using our anisotropic GB-PSDM (Fig. 8b) shows that the flat reflector is well focused and positioned. The image of the thrust sheet is correct, and the defocusing artifacts around it are also eliminated. The test results clearly demonstrate that our anisotropic GB-PSDM substantially improves the quality of converted PS-wave imaging compared with the isotropic algorithm.

6. Conclusions

We developed an anisotropic Gaussian beam prestack depth migration method for converted PS-wave in the common shot domain. The method builds on the ray tracing of P- and SV-waves that we derive for use in two-dimensional TI media. The ray tracing system is quite similar for P- and SV-waves in anisotropic media, and the type of wave whose ray is to be computed is specified by the initial conditions. The impulse responses of P- and SV-propagation modes in TI media with both vertical and tilted symmetry axes demonstrate the accuracy of the derived P- and SV-waves ray tracing.

Because S-waves are typically influenced more by anisotropy in a medium than are P-waves, the anisotropy has a large influence on the accuracy of converted PS-wave image. Our anisotropic migration algorithm can obtain accurate converted PS-wave images of subsurface structures in anisotropic media. In principle, the method is suitable for any strength of anisotropy. Tests of numerical examples illustrated that our anisotropic GB-PSDM method of converted PS-wave is

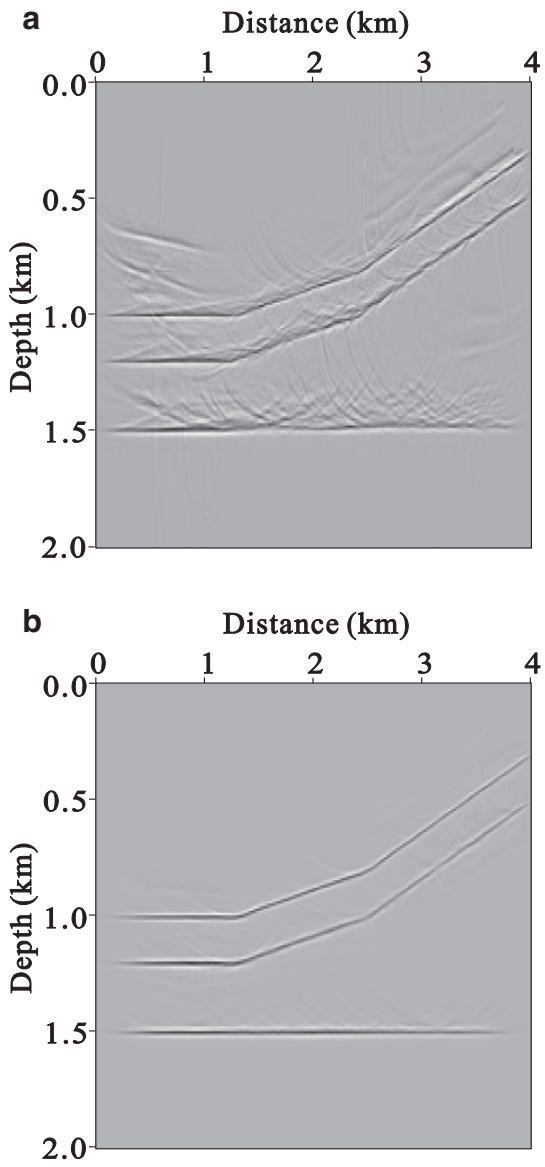

Fig. 8. Migration results of TTI media model (Fig. 6) using (a) the isotropic GB-PSDM and (b) anisotropic GB-PSDM. Anisotropic migration provides a correct image, and the events exactly fit the interfaces.

effective and that it is a good choice for converted PS-wave imaging in anisotropic media.

Acknowledgments

This research is supported by the National Special Fund of China (no. 2011ZX05035-001-006HZ, 2011ZX05008-006-22, 2011ZX05049-01-02, 2011ZX05019-003), the National Natural Science Foundation of China (no. 41104084), and the PetroChina Innovation Foundation (no. 2011D-5006-0303).

References

Alkhalifah, T., 1995. Gaussian beam depth migration for anisotropic media. Geophysics 60, 1474–1484. http://dx.doi.org/10.1190/1.1443881.
Alkhalifah, T., Larner, K., 1994. Migration error in transversely isotropic media. Geophysics 59, 1405–1418. http://dx.doi.org/10.1190/1.1443698.
Ball, G., 1995. Estimation of anisotropy and anisotropic 3D prestack depth migration, offshore, Zaire. Geophysics 60, 1495–1513. http://dx.doi.org/10.1190/1.1443883.
Bancroft, J.C., Geiger, H.D., Margrave, G.F., 1998. The equivalent offset method of prestack time migration. Geophysics 63, 2042–2053. http://dx.doi.org/10.1190/1.1444497.
Casasanta, L., Gray, S., Grion, S., 2013. Converted-wave controlled beam migration with sparse sources or receivers. 75th Conference and Exhibition, EAGE, Extended Abstracts.
Červeny, V., 1972. Seismic rays and ray intensities in inhomogeneous anisotropic media. Geophys. J. R. Astron. Soc. 29, 1–13. http://dx.doi.org/10.1111/j.1365-246X.1972.tb06147.x.
Červeny, V., 1985. Gaussian beams synthetic seismograms. J. Geophys. 58, 44–72.
Červeny, V., 2001. Seismic Ray Theory. Cambridge University Press, Cambridge.
Červeny, V., Popov, M.M., Psencik, I., 1982. Computation of wave fields in inhomogeneous media-Gaussian beam approach. Geophys. J. R. Astron. Soc. 70, 109–128. http://dx.doi.org/10.1111/j.1365-246X.1982.tb06394.x.
Červeny, V., Klimes, L., Psencik, I., 2007. Seismic ray method: recent developments. Adv. Geophys. 48, 1–126.
Crampin, S., Chesnokov, E.M., Hipkin, R.G., 1984. Seismic anisotropy — the state of the art: II. Geophys. J. R. Astron. Soc. 76, 1–16. http://dx.doi.org/10.1111/j.1365-246X.1984.tb05017.x.
Dai, H.C., Li, X.Y., 2006. The effects of migration velocity errors on traveltime accuracy in prestack Kirchhoff time migration and the image of PS converted waves. Geophysics 71, S73–S83. http://dx.doi.org/10.1190/1.2187788.
Du, X., Bancroft, J.C., Lines, L.R., 2007. Anisotropic reverse time migration for tilted TI media. Geophys. Prospect. 55, 853–869. http://dx.doi.org/10.1111/j.1365-2478.2007.00652.x.
Gray, S.H., 2005. Gaussian beam migration of common-shot records. Geophysics 70, S71–S77. http://dx.doi.org/10.1190/1.1988186.
Gray, S.H., Bleistein, N., 2009. True-amplitude Gaussian-beam migration. Geophysics 74, S11–S23. http://dx.doi.org/10.1190/1.3052116.
Hale, D., 1992a. Migration by the Kirchhoff, slant stack and Gaussian beam methods. Colorado School of Mines Center for Wave Phenomena Report 121.
Hale, D., 1992b. Computational aspects of Gaussian beam migration. Colorado School of Mines Center for Wave Phenomena Report 139.
Han, B., 2000. Two prestack converted-wave migration algorithms for vertical transverse isotropy. 70th Annual International Meeting, SEG, Expanded Abstracts, pp. 461–464.
Hanyga, A., 1986. Gaussian beams in anisotropic elastic media. Geophys. J. R. Astron. Soc. 85, 473–503.
Hill, N.R., 1990. Gaussian beam migration. Geophysics 55, 1416–1428. http://dx.doi.org/10.1190/1.1442788.
Hill, N.R., 2001. Prestack Gaussian-beam depth migration. Geophysics 66, 1240–1250. http://dx.doi.org/10.1190/1.1487071.
Isaac, J.H., Lawton, D.C., 1999. Image mispositioning due to dipping TI media; a physical seismic modeling study. Geophysics 64, 1230–1238. http://dx.doi.org/10.1190/1.1444629.
Kendall, R.R., Gray, S.H., Murphy, G.E., 1998. Subsalt imaging using prestack depth migration of converted waves: Mahogany field, Gulf of Mexico. 68th Annual International Meeting, SEG, Expanded Abstracts, pp. 2052–2055.
Kumar, D., Sen, M.K., Ferguson, R.J., 2004. Traveltime calculation and prestack depth migration in tilted transversely isotropic media. Geophysics 69, 37–44. http://dx.doi.org/10.1190/1.1649373.
Larner, K., Cohen, J.K., 1993. Migration error in transversely isotropic media with linear velocity variation in depth. Geophysics 58, 1454–1467. http://dx.doi.org/10.1190/1.1443360.
Levin, F.K., 1979. Seismic velocities in transversely isotropic media. Geophysics 44, 918–936. http://dx.doi.org/10.1190/1.1440985.
Li, X.Y., Dai, H., Mancini, F., 2007. Converted-wave imaging in anisotropic media: theory and case studies. Geophys. Prospect. 55, 345–363. http://dx.doi.org/10.1111/j.1365-2478.2007.00612.x.
Miao, X.G., Torre, Z., 2007. Anisotropic velocity updating for converted-wave prestack time migration. Geophysics D29–D32. http://dx.doi.org/10.1190/1.2435172.
Miao, X., Gray, S., Zhang, Y., Kendall, R., 2005. Converted-wave true amplitude prestack Kirchhoff migration. 75th Annual International Meeting, SEG, Expanded Abstracts, pp. 935–938.
Nolte, B., 2005. Converted-wave migration for VTI media using Fourier finite-difference depth extrapolation. 67th Conference and Exhibition, EAGE, Extended Abstracts, p. P001.
Nowack, R.L., 2003. Calculation of synthetic seismograms with Gaussian beams. Pure Appl. Geophys. 160, 487–507 (doi: 0033-4553/03/040487-21).
Pedersen, Ø., Ursin, B., Helgesen, H.K., 2010. One-way wave-equation migration of compressional and converted waves in a VTI medium. Geophysics 75, S237–S248. http://dx.doi.org/10.1190/1.3509466.
Popov, M.M., 1982. A new method of computation of wave fields using Gaussian beams. Wave Motion 4, 85–97.
Popov, M.M., Semtchenok, N.M., Popov, P.M., Verdel, A.R., 2008. Reverse time migration with Gaussian beams and velocity analysis applications. 70th Conference and Exhibition, EAGE, Extended Abstracts, p. F048.
Popov, M.M., Semtchenok, N.M., Popov, P.M., Verdel, A.R., 2010. Depth migration by the Gaussian beam summation method. Geophysics 75, S81–S93. http://dx.doi.org/10.1190/1.3361651.
Sena, A.G., Toksöz, M.N., 1993. Kirchhoff migration and velocity analysis for converted and nonconverted waves in anisotropic media. Geophysics 58, 265–276. http://dx.doi.org/10.1190/1.1443411.
Stewart, R.R., Gaiser, J.E., Brown, R.J., Lawton, D.C., 2002. Converted wave seismic exploration: methods. Geophysics 67, 1348–1363. http://dx.doi.org/10.1190/1.1512781.
Stewart, R.R., Gaiser, J.E., Brown, R.J., Lawton, D.C., 2003. Converted wave seismic exploration: applications. Geophysics 68, 40–57. http://dx.doi.org/10.1190/1.1543193.
Sun, C.W., Martinez, R.D., 2003. 3D Kirchhoff PS-wave prestack time migration for V(z) and VTI media. 73th Annual International Meeting, SEG, Expanded Abstracts, pp. 957–960.

Sun, R., McMechan, G.A., 2001. Scalar reverse-time depth migration of prestack elastic seismic data. Geophysics 66, 1519–1527. http://dx.doi.org/10.1190/1.1487098.
Thomsen, L., 1986. Weak elastic anisotropy. Geophysics 51, 1954–1966. http://dx.doi.org/10.1190/1.1442051.
Thomsen, L., 1999. Converted-wave reflection seismology over inhomogeneous, anisotropic media. Geophysics 64, 678–690. http://dx.doi.org/10.1190/1.1444577.
Tsvankin, I., Gaiser, J., Grechka, V., Baan, M.V.D., Thomsen, L., 2010. Seismic anisotropy in exploration and reservoir characterization: an overview. Geophysics 75, A15–A29. http://dx.doi.org/10.1190/1.3481775.
Vestrum, R.W., Lawton, D.C., Schmid, R., 1999. Imaging structures below dipping TI media. Geophysics 64, 1239–1246. http://dx.doi.org/10.1190/1.1444630.
Wang, Z.J., 2002. Seismic anisotropy in sedimentary rocks, part 2: laboratory data. Geophysics 67, 1423–1440. http://dx.doi.org/10.1190/1.1512743.
Wang, W.Z., Pham, L.D., Min, L., 2002. Converted wave prestack time migration for isotropic and anisotropic media. 72th Annual International Meeting, SEG, Expanded Abstracts, pp. 990–993.
Wang, Y., Wang, W., Yin, J.J., 2012. A modified EOM method for PS-wave migration. Explor. Geophys. 43, 156–161. http://dx.doi.org/10.1071/EG11019.
White, J.E., Martineau-Nicoletis, L., Monash, C., 1983. Measured anisotropy in Pierre shale. Geophys. Prospect. 31, 709–725. http://dx.doi.org/10.1111/j.1365-2478.1983.tb01081.x.
Winterstein, D.F., 1990. Velocity anisotropy terminology for geophysicists. Geophysics 55, 1070–1088. http://dx.doi.org/10.1190/1.1442919.
Xie, X.B., Wu, R.S., 2005. Multicomponent prestack depth migration using the elastic screen method. Geophysics 70, S30–S37. http://dx.doi.org/10.1190/1.1852787.
Zhang, L.Y., Liu, Y., 2008. Anisotropic converted wave amplitude-preserving prestack time migration by the pseudo-offset method. Appl. Geophys. 5, 204–211. http://dx.doi.org/10.1007/s11770-008-0030-6.
Zhang, J.F., Verschuur, D.J., Wapenaar, C.P.A., 2001. Depth migration of shot records in heterogeneous, transversely isotropic media using optimum explicit operators. Geophys. Prospect. 49, 287–299. http://dx.doi.org/10.1046/j.1365-2478.2001.00255.x.
Zhang, Y., Zhang, H.Z., Zhang, G.Q., 2011. A stable TTI reverse time migration and its implementation. Geophysics 76, WA3–WA11. http://dx.doi.org/10.1190/1.3554411.
Zhu, X., Langhammer, J., King, D., Madtson, E., Helgesen, H.K., Brzostowski, M., 1999. Converted-wave pre-stack depth migration of North Sea salt domes. 69th Annual International Meeting, SEG, Expanded Abstracts, pp. 1087–1090.
Zhu, T.F., Gray, S.H., Wang, D.L., 2007. Prestack Gaussian-beam depth migration in anisotropic media. Geophysics 72, S133–S138. http://dx.doi.org/10.1190/1.2711423.